

Layer thickness dependent plastic deformation mechanism in Ti/TiCu dual-phase nano-laminates

Minrong An(安敏荣), Yuefeng Lei(雷岳峰), Mengjia Su(宿梦嘉), Lanting Liu(刘兰亭), Qiong Deng(邓琼), Haiyang Song(宋海洋), Yu Shang(尚玉), and Chen Wang(王晨)

Citation: Chin. Phys. B, 2023, 32 (**6**): 066201. DOI: 10.1088/1674-1056/acb48f
Journal homepage: http://cpb.iphy.ac.cn; http://iopscience.iop.org/cpb

What follows is a list of articles you may be interested in

Molecular dynamics simulation of interaction between nanorod and phospholipid molecules bilayer

Xin Wang(王鑫), Xiang-Qin Li(李香琴), Tian-Qing Liu(刘天庆), Li-Dan Zhao(赵丽丹), Ke-Dong Song(宋克东), and Dan Ge(葛丹)

Chin. Phys. B, 2023, 32 (**1**): 016201. DOI: 10.1088/1674-1056/ac6ed8

Effect of void size and Mg contents on plastic deformation behaviors of Al-Mg alloy with pre-existing void: Molecular dynamics study

Ning Wei(魏宁), Ai-Qiang Shi(史爱强), Zhi-Hui Li(李志辉), Bing-Xian Ou(区炳显), Si-Han Zhao(赵思涵), and Jun-Hua Zhao(赵军华)

Chin. Phys. B, 2022, 31 (**6**): 066203. DOI: 10.1088/1674-1056/ac4a74

Nonperturbative effects of attraction on dynamical behaviors of glass-forming liquids

Xiaoyan Sun(孙晓燕), Haibo Zhang(张海波), Lijin Wang(王利近), Zexin Zhang(张泽新), and Yuqiang Ma(马余强)\ccclink

Chin. Phys. B, 2020, 29 (**12**): 126201. DOI: 10.1088/1674-1056/abbbdd

Balancing strength and plasticity of dual-phase amorphous/crystalline nanostructured Mg alloys

Jia-Yi Wang(王佳怡), Hai-Yang Song(宋海洋), Min-Rong An(安敏荣), Qiong Deng(邓琼), Yu-Long Li(李玉龙)

Chin. Phys. B, 2020, 29 (**6**): 066201. DOI: 10.1088/1674-1056/ab84d5

Anisotropic plasticity of nanocrystalline Ti: A molecular dynamics simulation

Minrong An(安敏荣), Mengjia Su(宿梦嘉), Qiong Deng(邓琼), Haiyang Song(宋海洋), Chen Wang(王晨), Yu Shang(尚玉)

Chin. Phys. B, 2020, 29 (**4**): 046201. DOI: 10.1088/1674-1056/ab7188

Layer thickness dependent plastic deformation mechanism in Ti/TiCu dual-phase nano-laminates

Minrong An(安敏荣)[1], Yuefeng Lei(雷岳峰)[3], Mengjia Su(宿梦嘉)[2], Lanting Liu(刘兰亭)[2], Qiong Deng(邓琼)[2,†], Haiyang Song(宋海洋)[1,‡], Yu Shang(尚玉)[1], and Chen Wang(王晨)[4]

[1] *College of New Energy, Xi'an Shiyou University, Xi'an* 710065, *China*
[2] *Fundamental Science on Aircraft Structural Mechanics and Strength Laboratory, Northwestern Polytechnical University, Xi'an* 710072, *China*
[3] *School of Materials Science and Engineering, Northwestern Polytechnical University, Xi'an* 710072, *China*
[4] *College of Materials Science and Engineering, Xi'an Shiyou University, Xi'an* 710065, *China*

(Received 8 September 2022; revised manuscript received 15 January 2023; accepted manuscript online 19 January 2023)

Crystalline/amorphous nanolaminate is an effective strategy to improve the mechanical properties of metallic materials, but the underlying deformation mechanism is still under the way of exploring. Here, the mechanical properties and plastic deformation mechanism of Ti/TiCu dual-phase nanolaminates (DPNLs) with different layer thicknesses are investigated using molecular dynamics simulations. The results indicate that the influence of the layer thickness on the plastic deformation mechanism in crystalline layer is negligible, while it affects the plastic deformation mechanism of amorphous layers distinctly. The crystallization of amorphous TiCu is exhibited in amorphous parts of the Ti/TiCu DPNLs, which is inversely proportional to the layer thickness. It is observed that the crystallization of the amorphous TiCu is a process driven by stress and heat. Young's moduli for the Ti/TiCu DPNLs are higher than those of composite material due to the amorphous/crystalline interfaces. Furthermore, the main plastic deformation mechanism in crystalline part: grain reorientation, transformation from hexagonal-close-packed-Ti to face-centered cubic-Ti and body-centered cubic-Ti, has also been displayed in the present work. The results may provide a guideline for design of high-performance Ti and its alloy.

Keywords: dual-phase nanolaminate, molecular dynamics simulation, deformation mechanism, crystallization

PACS: 62.25.–g, 31.15.xv, 61.82.Rx

DOI: 10.1088/1674-1056/acb48f

1. Introduction

Titanium (Ti) and its alloys, as a kind of "future metal", exhibit various excellent properties including high corrosion resistance, high strength, and biological compatibility.[1–4] However, the tradeoff of strength and ductility in Ti restricts the application of the Ti and its alloy. In the past decades, a variety of technological pathways for effectively mechanical properties of metallic materials have been developed including hierarchical nanotwinned structures, extreme grain refinement, dislocation architectures[5,6] and nanolaminate structures.[7,8] Especially, the nanolaminate structures can possess the advantages of the components used in the nanolaminates, and even obtain some unexpected achievements.[9–14] For example, the nanotwinned Al/Ti multilayers exhibited compressive strength up to 2.4 GPa, good hardness and work hardening capability, which was much higher than the pure Ti and Al.[12] In addition, the annealed Al/Ti nanolaminates possessed high flow stress (exceeding 3 GPa), work hardening capability, and good deformability.[13] The crystalline/crystalline interface (CCI) plays an important role in the improvement of the mechanical properties of the nanolaminates, but the stress often concentrates in the interphase interface, which may induce the nano-void in nanolaminates.

Recently, the crystalline/amorphous interface (ACI) has been introduced into the nanolaminates, in which the amorphous alloy is taken as the components of the nanolaminates. The crystalline/amorphous nanolaminates were reported to be an effective strategy to improve the strength and ductility simultaneously.[15] As is known to all, amorphous alloy is also called metallic glasses (MGs). There is neither dislocation slip nor twin during the plastic deformation, which results in the catastrophic fracture of MGs at room temperature.[15–18] However, on the one hand, the dislocations emitted from the crystalline phase will be absorbed by the ACI infinitely. On the other hand, the shear transformation zones or shear band in amorphous phase are inhibited by the ACI. The crystalline phase, amorphous phase, and ACI will affect the mechanical properties of the nanolaminate cooperatively.[16–18] Wang *et al.*[15] prepared the Cu/CuZr crystalline/amorphous multilayers and found that the nanolaminates exhibited a high flow stress of nearly 1.09 GPa, as well as a nearly elastic-perfectly plastic behavior without necking. The tensile elongation to failure around 13.8%, which was 6–8 times higher than that typically observed in conventional crystalline/crystalline nanolaminates ($< 2\%$) and most other nanocrystalline materi-

†Corresponding author. E-mail: dengqiong24@nwpu.edu.cn
‡Corresponding author. E-mail: hysong@xsyu.edu.cn

© 2023 Chinese Physical Society and IOP Publishing Ltd

als. Zhang and his coworkers performed a lot of work to investigate the mechanical properties of crystalline/amorphous nanolaminates.[19–24] They pointed out that the mechanical properties of Cu/Cu–Zr crystalline/amorphous are dependent on the diameter of the sample, the modulation ratio η and the layer thickness.[19,22] In crystalline/amorphous Cu/Ta nanolaminates, the hardness increases monotonically with decreasing of η, however, there is an unexpected hardening to softening when the η changes.[24] The Ag/Cu–Zr nanolaminates show that the tensile ductility firstly decreases and subsequently increases with raising η.[20] However, the Mo/Cu–Zr nanolaminates exhibit a different η-dependence where the tensile ductility monotonically increases with η.[20] The results mentioned above indicate that the mechanical properties and deformation mechanism of the nanolaminates are dependent on the layer thickness. However, the relation of the layer thickness to the strengthening and toughening mechanism is still under the way of exploring.

Copper, due to its physical and chemical properties such as good electrical conductivity, thermal conductivity, corrosion resistance and ductility, is widely used in electrical industry, machinery manufacturing, etc. Especially, the combination of Cu and Ti makes Cu–Ti films used widely in microelectronics, surface acoustic wave technology,[25] semi-solid processing,[26] and biomedicine.[27] As one kind of functional materials, Cu–Ti based alloy has excellent mechanical properties, such as extreme hardness, good sound absorption, and electric conductivity.[28] B2 phase is often observed in TiCu-based metallic glasses, representing obvious plastic deformation and pronounced work hardening behavior after yielding during compression as well as tension process, which attracts more attention in recent years.[29,30] In view of this, the mechanical properties of crystalline/amorphous Ti/TiCu dual-phase nanolaminates (DPNLs) are investigated in this work.

Generally speaking, the mechanical properties of macroscopic materials are investigated by tension, compression, shear, and torsion. However, when the material size is reduced to the nanoscale, it is difficult to test the mechanical properties of nanomaterials by macroscopic means. For nanomaterials, we often employ nano-indentation,[31] nano-scratch,[32] nano-imprint,[33] and micro-column compression[34] to measure their mechanical properties in nanoscale. However, there are rare studies on the tensile mechanical properties of metallic nano-multilayers perpendicular to the interfaces. Under the restriction by the modern experimental and electron microscopic technology, it is difficult to capture the detailed evolution process of microstructure. The mechanism responsible for the deformation process of metallic nano-multilayers needs to be further clarified. In addition to experimental studies, numerical simulation methods are a very attractive and useful tool for studying material properties and have been widely used to investigate the strengthening and fracture mechanisms of nanolayered materials. Molecular dynamics (MD) simulation provides an alternative method to experiments, which plays an important role in understanding the deformation mechanism in metallic materials.[35–38] Actually, the mechanical properties of the crystalline/amorphous nanolaminates have been investigated in the past few years using MD simulation.[39–42] Tran and Fang[39] reported that the plastic deformation zones increase as the thickness of each layer decreases in crystalline/amorphous Cu/CuTa nanolaminates. For Cu/CuZr nanolaminates with equal layer thickness of crystalline phase and amorphous phase, a transition in the plastic deformation mode takes place from homogeneous plastic co-deformation between interfacial dislocation and shear transformation zones to multiple shear bands interaction.[40] For the crystalline/amorphous Mg/MgAl nanolaminates,[41,42] the plastic deformation mechanism is dependent on the orientation of the crystalline part and the layer thickness of the candidates in nanolaminates. Especially, the reorientation and formation of basal/prismatic interface have been observed as the new plastic deformation mechanism in Mg crystal, which also influences the mechanical properties of Mg/MgAl nanolaminates. Different from the deformation models in hexagonal-close-packed (HCP) metals Mg, there are six types of twins in deformed HCP structure Ti[43,44] including tensile twins of $\{11\bar{2}1\}\langle 11\bar{2}6\rangle$, $\{10\bar{1}2\}\langle 10\bar{1}1\rangle$, and $\{11\bar{2}3\}\langle 33\bar{6}2\rangle$, as well as compressive twins of $\{10\bar{1}1\}\langle 10\bar{1}2\rangle$, $\{11\bar{2}2\}\langle 11\bar{2}3\rangle$, and $\{11\bar{2}4\}\langle 22\bar{4}3\rangle$. Thus, whether the relation between the mechanism and the layer thickness mentioned above can be applied to Ti-based crystalline/amorphous nanolaminates is not clear.

In the present work, the effect of layer thickness on the mechanical properties of crystalline/amorphous Ti/TiCu dual-phase nanolaminates (DPNLs) is investigated by MD simulation at 300 K. The results indicate that the layer thickness affects the plastic deformation mechanism of crystalline layer negligibly, while it may influence the deformation in amorphous layers dramatically. It is interesting is that the crystallization of the amorphous is observed in DPNLs. The results obtained in this work may provide a guidance for designs and applications of high-performance Ti-based MG and multilayered composites.

2. Simulation model and method

The schematic of Ti/TiCu DPNLs under tension loading is depicted in Fig. 1, in which the crystalline Ti layer and amorphous TiCu layer are arranged alternately. The thicknesses of crystalline Ti layer and amorphous TiCu layer along Y direction are equal. For creating these crystalline/amorphous DPNLs, the TiCu amorphous alloy is constructed firstly. The process can be divided into three steps as follows: (I) The initial TiCu alloy model is constructed containing 49977 Ti atoms and 48807 Cu atoms. (II) The TiCu alloy is heated at 1200 K

till to the liquid state. (Ⅲ) The liquid alloy is quenched from 1200 K to 50 K at a cooling rate of 2×10^{12} K/s for 60 ps to eliminate thermal fluctuations of the system. Periodic boundary conditions (PBCs) are applied along all three directions in this process. Radial distribution function (RDF) is often used to describe the structural ordering of materials. Generally, the RDF of the crystalline structure displays the sharp peaks, while it shows a split in the second peak and subsequent flat peaks for the amorphous alloy.[45] The RDFs in Fig. 1 indicate that the crystalline Ti and amorphous TiCu alloy are established well in the present work. The crystalline Ti is assigned as $\langle \bar{1}010 \rangle$ along X direction, $\langle 0001 \rangle$ along Y direction, and $\langle \bar{1}2\bar{1}0 \rangle$ along Z direction. The $\langle 0001 \rangle$ direction is perpendicular to the crystalline/amorphous interfaces, which is built according to the Ti-based nano-multilayers obtained in experiment.[9,13] The details of the crystalline Ti are shown in the inserted picture in the upper right corner of Fig. 1. The stacking sequence of atomic planes is ABABAB$\cdots$ along Y direction, which is the close-packed structure. The ACI is formed at the junction region due to the different structures. The crystalline/amorphous Ti/TiCu structure is then replicated for 8, 6, 5, 4, 3, and 2 times to form a multilayered composite, in which the layer thickness d for crystalline phase and amorphous phase increases equally from 3.76 nm to 15.03 nm. The dimensions for the samples are 5.4 nm $\times$ 59.8 nm $\times$ 16.4 nm in the X, Y, and Z directions, which contains $\sim$ 340000 atoms.

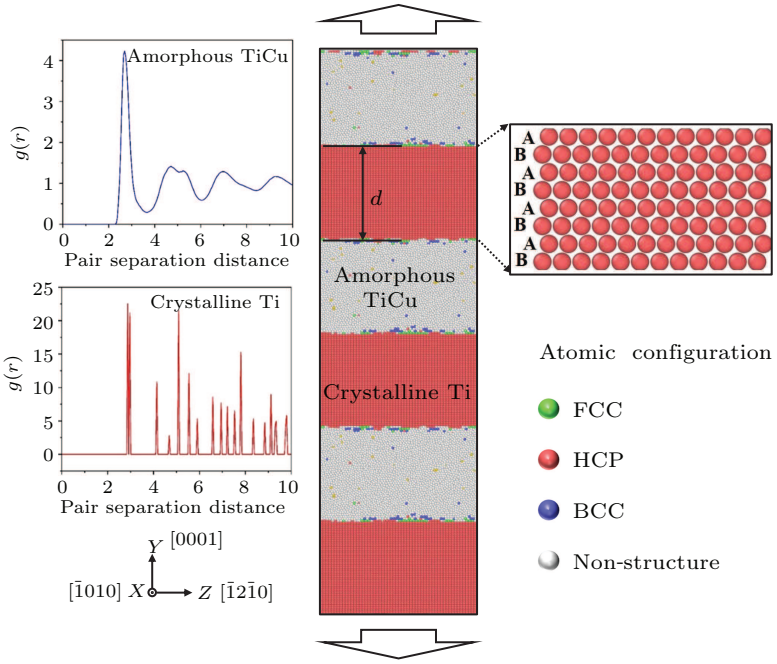


Fig. 1. The schematic of Ti/TiCu dual-phase nanolaminates (DPNLs). The radial distribution functions of disparate phases are shown in left part. The insert picture in the upper right corner depicts the stacking sequence of the crystalline Ti. The different types of atoms are displayed in the lower right corner.

All MD simulations are performed by using the large-scale atomic/molecular massively parallel simulator (LAMMPS).[46] The EAM potential in the MD simulation is developed by Wadley and Zhou,[47,48] which is adopted to describe Ti–Ti, Ti–Cu, and Cu–Cu interatomic interactions in the simulation models. The potential is well fitted to the basic material properties such as lattice constants, elastic constants, bulk moduli, vacancy formation energies, and sublimation energies, which has been performed to investigate the mechanical and thermal properties of materials[49,50] for many times. The simulation temperature is set as 300 K. Periodic boundary condition is applied in all three directions. Prior to loading, the structure is equilibrated for 100 ps in the isothermal-isobaric (NPT) ensemble to equilibrate the interface structures and eliminate the local defects. Subsequently, tension loading is applied along Y direction at the strain rate of 5×10^8 s^{-1} with a time step of 2 fs. The common neighbor analysis (CNA)[51] is used to visualize the microstructure of the crystalline Ti, in which the HCP atoms, body-centered cubic (BCC) atoms, face-centered cubic (FCC) atoms and non-structure atoms are colored red, blue, green and white gray, respectively. The shear von Mises strain (η^{Mises})[52] is also selected to quantify the mechanical responses of amorphous layers. They are implemented in the software of the open visualization tool (OVITO).[53]

3. Results and discussion

3.1. Mechanical behavior of the Ti/TiCu DPNLs

The stress–strain curves of the Ti/TiCu DPNLs with different layer thicknesses, as well as the crystalline Ti and amorphous TiCu, are shown in Fig. 2(a). It is observed from Fig. 2(a) that the stresses of the Ti/TiCu DPNLs increase proportionally with the increase of strain at the initial tensile stage. Subsequently, the stresses show a slight increase and

decrease with strain up. Compared with the Ti/TiCu DPNLs, the peak stress and elastic modulus of the crystalline Ti are the largest, while of the amorphous TiCu are the lowest. The results imply that the introduction of crystalline Ti to the amorphous phase is an effective way to improve the Young's modulus and the strength of the MG. Figure 2(b) demonstrates the variation of Young's modulus for the samples in this work, in which the values are between the crystalline Ti ($E_{\rm Ti}$ = 124.91 GPa) and the amorphous TiCu ($E_{\rm A} = 32.57$ GPa). Furthermore, Young's moduli for the Ti/TiCu DPNLs are higher than the value obtained by the role of mixture of composite materials [the pink dotted line in Fig. 2(b)].[54]

$$E_{\rm Rom} = \left(\frac{V_{\rm Ti}}{E_{\rm Ti}} + \frac{V_{\rm TiCu}}{E_{\rm TiCu}}\right)^{-1}, \tag{1}$$

where $E_{\rm Ti}$ and $E_{\rm TiCu}$ are the elastic moduli of crystllilne Ti and amorphous TiCu, respectively. $V_{\rm Ti}$ and $V_{\rm TiCu}$ are the relative volume fractions, which should satisfy $V_{\rm Ti} + V_{\rm TiCu} = 1$. The result is consistent with the conclusion in Ag/Fe multilayers.[55] However, Young's modulus for the Ti/TiCu DPNLs increases slightly with the increase of the layer thickness, which is different from the result obtained in Ti/Ni nano-multilayers.[56] The reason may be that the ACIs are more inclusive compared with the CCIs. The mechanical behavior of the Ti/TiCu DPNLs is affected by the three parts: crystalline Ti layer, TiCu amorphous layer, and ACIs. There are more ACIs in the samples with smaller layer thickness. The more the ACIs, the more the interface atoms. The variation of the interface atom fraction with layer thickness has been exhibited in Fig. 2(b). ACI atoms are the 3–4 layers' atoms in the interfaces between the crystalline phase and the amorphous phase, in which the ACI thickness is identified by the results of the CNA method. If the atoms in the crystalline parts do not belong to the HCP structure totally in one layer, or there are crystalline atoms in the amorphous parts near the ACI in one layer, then the atoms are defined as the ACI atoms. When the tensile loading is applied, stress concentration occurs in the junctions of crystalline part and amorphous part firstly, i.e., ACIs. The initial plastic deformation of DPNLs initiates from the interfacial regions. When the layer thickness is 3.76 nm, the fraction of the ACI atoms is up to 16.7%. The ACIs may bear certain of the elastic deformation. When the layer thickness is increased to 15.03 nm, the fraction of ACI atoms is just 3.4%. Most part of the elastic deformation is undertaken by the crystalline and amorphous parts, while the softening effect of the ACIs is relatively small. This is why Young's modulus for the Ti/TiCu DPNLs increases with the increase of the layer thickness.

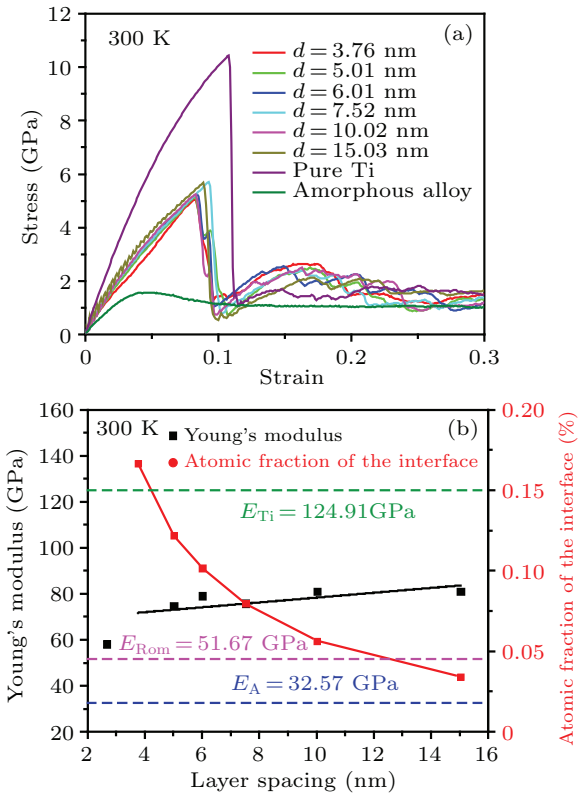


Fig. 2. (a) Stress–strain curves of Ti/TiCu DPNLs with different layer thicknesses. The crystalline Ti and amorphous TiCu are also shown for comparison. (b) The variation of Young's modulus and atom fraction of interface versus layer thickness.

In order to clarify the relations between the deformation mechanism and the layer thickness, Figs. 3–5 show the microstructure evolution of the Ti/TiCu DPNLs with different layer thicknesses. The atomic configurations of the crystalline layers are analyzed by the CNA method, while the amorphous layers are analyzed by atomic shear strain only in Figs. 3(a)–3(d) and the CNA method only in enlarged snapshots of A, B and C. The crystalline layers are long-ranged and orderly structure, and the orderly structures are presented in HCP, FCC and BCC structures generally upon the CNA results. Nevertheless, the shear transformation zones are the embryos of the shear bands in metallic glass, which are long-range disorder and defined as the large atomic strain cluster bearing local events of cooperative shearing and realigning to a more astable state.[57] Thus, the typical structure of the shear transformation zones is non-structure indicated by the white gray atoms according to the CNA results.

Figure 3 demonstrates the evolution of the atomic configurations for the Ti/TiCu DPNL with a smaller layer thickness of 3.76 nm. It is observed from Figs. 3(a) and 3(b) that some shear transformation zones (STZs) are formed in the amorphous phase at the linear stage of stress–strain curves shown in Fig. 2(a). A new grain generates at the strain of 0.084, which corresponds to the yield of the crystalline Ti in Ti/TiCu DPNL. It indicates that the yield of the crystalline Ti leads to the drop of the stress shown in Fig. 2(a), and the TiCu amorphous phase comes to the plastic stage earlier than the crystalline

part. With further loading, more new grains containing FCC stacking faults (SFs) occur in the Ti layers, and the new grains grow up constantly. The grain boundaries of the new grains are blocked and absorbed by the adjacent ACIs, as shown in Fig. 3(c). Some BCC atoms appear in the Ti layers, i.e., the HCP-Ti transforms to BCC-Ti in the tensile process, as shown in Fig. 3(d). There is no shear band forming in the amorphous layers during the deformation, which indicates that the amorphous layers undergo uniform plastic deformation. Moreover, it is interesting that some BCC atoms emerge in the amorphous TiCu layers, implying the crystallization of amorphous TiCu phase. The evolution of the BCC atoms is presented in the top right corner of Fig. 3. It is observed from the zoomed-up pictures of region A, B, and C that the BCC atoms initiate from the ACIs of the Ti/TiCu DPNL, and the BCC regions expand continuously with the tensile strain increasing. Nearly all of the TiCu amorphous phase has transformed to the BCC structure at $\varepsilon = 0.279$.

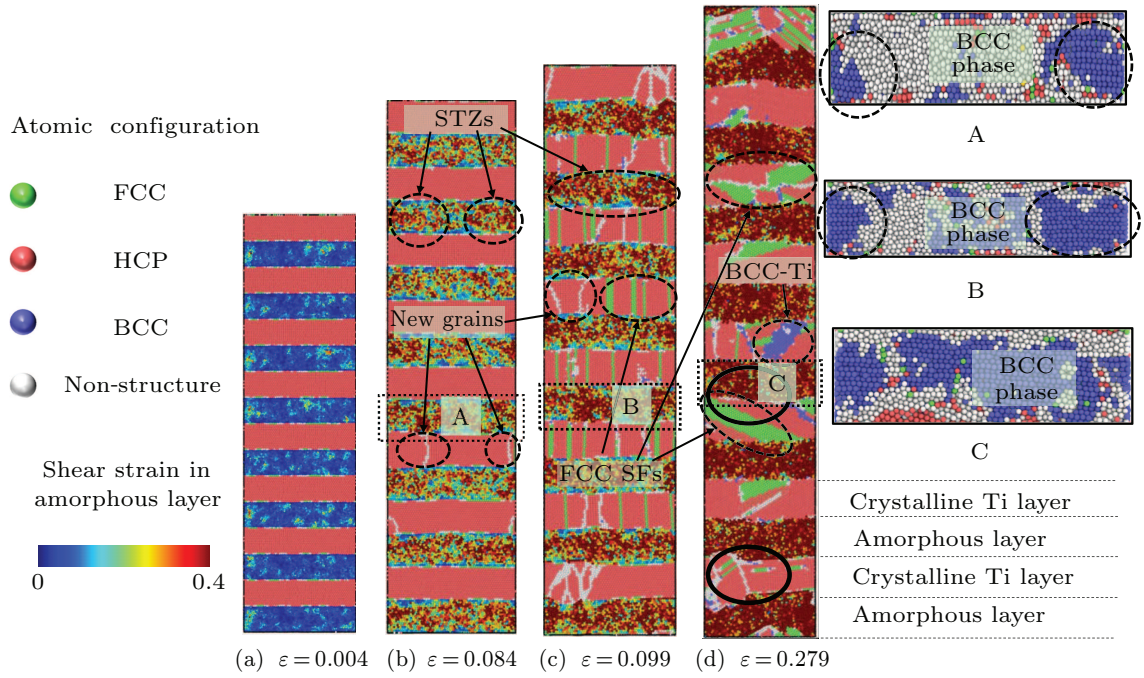


Fig. 3. The atomic configurations of the Ti/TiCu DPNL with $d = 3.76$ nm at different tensile strains. The pictures in the top right corner depict enlarged structures during the tensile process. In the panel, the atomic configurations of the crystalline layer are analyzed by the CNA method, while the amorphous layers are analyzed by atomic shear strain only in (a)–(d) and the CNA method only in enlarged snapshots of A, B, and C.

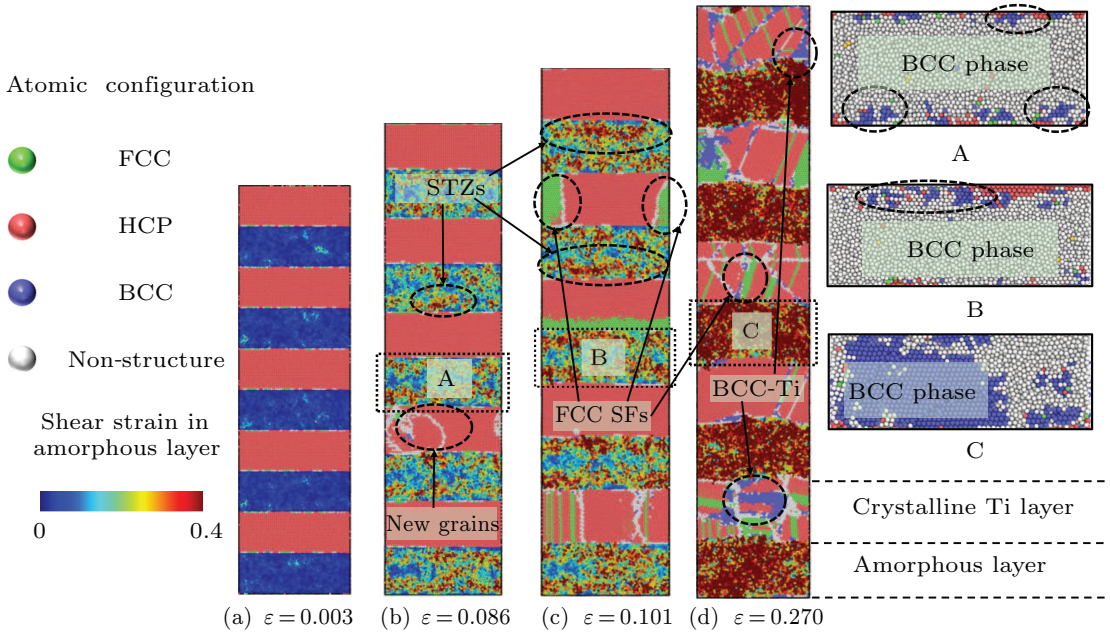


Fig. 4. The atomic configurations of the Ti/TiCu DPNL with $d = 6.01$ nm at different tensile strains. The magnified pictures in the top right corner illustrate the details of region A, B, and C enclosed by a black rectangle. In the panel, the atomic configurations of the crystalline layer are analyzed by the CNA method, while the amorphous layers are analyzed by atomic shear strain only in (a)–(d) and the CNA method only in enlarged snapshots of A, B, and C.

Figures 4 and 5 depict the evolution of the atomic configurations of the Ti/TiCu DPNL with a moderate layer thickness of 6.01 nm and a larger layer thickness of 15.03 nm, respectively. Examination of Figs. 4 and 5 shows that the deformation process of the Ti/TiCu DPNLs is similar to that of the former cases ($d = 3.76$ nm). The plastic deformation in the crystalline layer is dominated by the generation of new grains, the generation of FCC SFs, and the transformation from HCP-Ti to BCC-Ti. While the amorphous layers undertake the homogeneous plastic deformation, the main deformation mechanism is the formation of STZs and the crystallization of amorphous phase. Furthermore, the effect of the layer thickness on the plastic deformation mechanism in the crystalline layer is negligible, while it affects the amorphous layer dramatically. The crystalized region of the amorphous TiCu decreases with the increase of layer thickness.

It is observed from Figs. 3–5 that the crystallization of amorphous TiCu phase occurs during the tension, and is strongly related to the layer thickness of candidates in DPNLs. To search for more details, Fig. 6 shows the snapshots of the Ti/TiCu DPNLs with $d = 3.76$ nm, 6.01 nm, and 15.03 nm at the strain of 0.3, in which the CNA method is applied to discern the different defect structures. It is observed from Fig. 6 that in the sample with the smallest layer thickness, almost all of the amorphous phase has transformed to crystalline BCC phase; for the largest layer thickness, the crystallization of amorphous phase to BCC structure is observed only in the atoms near the ACIs; the degree of crystallization for the sample with moderate layer thickness is between the former ones.

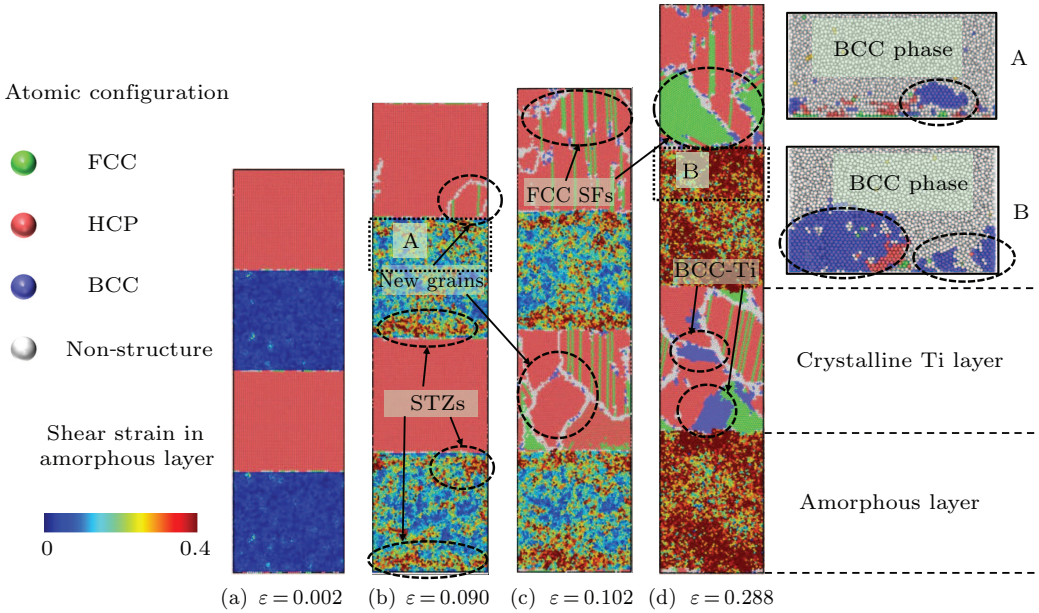


Fig. 5. The atomic configurations of the Ti/TiCu DPNL with $d = 15.03$ nm at different tensile strains. The magnified pictures in the top right corner show the details of regions A and B enclosed by a black rectangle. In the panel, the atomic configurations of the crystalline layers are analyzed by the CNA method, while the amorphous layers are analyzed by atomic shear strain only in (a)–(d) and the CNA method only in enlarged snapshots of A, B, and C.

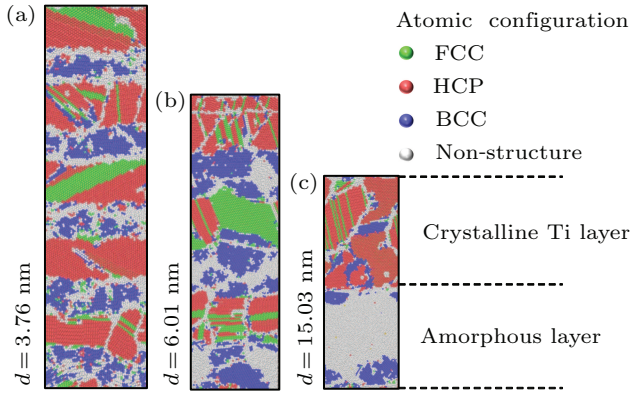


Fig. 6. Atomic configurations of the Ti/TiCu DPNLs with (a) $d = 3.76$ nm, (b) $d = 6.01$ nm, and (c) $d = 15.03$ nm at the strain of 0.3.

In order to illustrate the crystallization quantitatively, Fig. 7 presents the atomic fraction evolutions of different structures for Ti/TiCu DPNLs shown in Fig. 6. The difference values of HCP, BCC or FCC structure represent the extent to which the phase transition is progressing during the tension, while the variation of the non-structure atoms represents the degree of crystallization of amorphous phase. It is observed from Fig. 7(a) that the fraction of the amorphous atoms decreases from 51% to 27% while the fraction of BCC atoms increases from 2% to 24% between the strain range of 0–0.15 in the sample with layer thickness of 3.76 nm. In this process, the increase of FCC atoms is little and basically equal to the decrease of HCP atoms. It manifests that the crystallization from amorphous phase to the BCC structure is the main plastic deformation mechanism in this strain region. As the strain increases, the fractions of the amorphous phase and BCC atoms come to a constant value. However, the fraction of HCP atoms

decreases constantly, and the FCC atoms increase for complementarity. It indicates that the transformation from HCP-Ti to FCC-Ti in crystalline Ti is the main plastic deformation in this strain range. In the sample with moderate layer thickness of 6.01 nm, the increase of BCC atoms is on the cost of the decrease of amorphous phase when the strain is below 0.15, as shown in Fig. 7(b). When the tensile strain is larger than 0.15, the fractions of HCP and amorphous atoms decrease rapidly. The quantity of the FCC atoms keeps a constant value, while the fraction of the BCC atoms increases sharply. This implies that the main plastic deformation mechanism is BCC crystallization in amorphous phase and the transformation from HCP-Ti to BCC-Ti in crystalline Ti. However, for the sample with larger layer thickness, e.g., 15.03 nm (Fig. 7(c)), the decreasing amplitude of the amorphous phase is really small, indicating the limited crystallization region. It is in agreement with the results of Fig. 6(c), in which the crystallization of amorphous phase to the BCC structure is observed only in the atoms near the ACIs. In addition, the decrease of HCP atoms versus complementary increase of FCC atoms and BCC atoms is obvious in Fig. 7(c) when the strain is larger than 0.2, which indicates that the main deformation is the transformation from HCP-Ti to FCC-Ti and BCC-Ti. To sum up, the plastic deformation of the Ti/TiCu DPNLs is dominated by both the amorphous phase and crystalline phase, which is in agreement with the results obtained in Figs. 3–6.

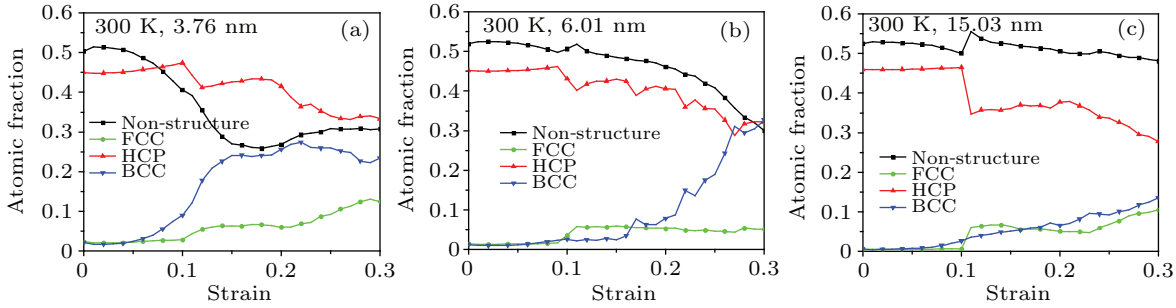


Fig. 7. Atomic fraction evolutions of different structures for Ti/TiCu DPNLs with layer thickness of (a) $d = 3.76$ nm, (b) $d = 6.01$ nm, and (c) $d = 15.03$ nm.

3.2. Plastic deformation mechanism in crystalline phase

We have presented that the plastic deformation for the Ti/TiCu DPNLs is dominated by both the crystalline phase and the amorphous phase. Figure 8 shows the details of the plastic deformation mechanism in crystalline phase. Examination of Fig. 8(a) shows that there are two kinds of crystallographic orientation between the matrix and the new grain, the basal/prismatic plane (BP plane, blue lines) and the inclined $\{10\bar{1}2\}\langle 10\bar{1}1\rangle$ twin boundary (TB, yellow lines), which arrange alternately to form the junction region of the matrix and the new grain. Actually, the basal plane of the new grain is rotated about 90° from basal plane of the matrix. Namely, the basal plane in the parent body transforms into the prismatic planes of the new lattice, creating the BP interface with misfit dislocations. Besides the BP plane, the $\{10\bar{1}2\}\langle 10\bar{1}1\rangle$ TB is also observed between the matrix and the new grains, in which the crystal orientation of the two sides differing by 84.78°. It is very close to the 90° angle between the two sides of the basal and prismatic plane. Therefore, this newly formed interface containing alternatively BP plane and TB can be regarded as a twin-like feature or grain reorientation, and the new grains is always called twin variant. This grain reorientation behavior has also been found in both simulation[58,59] and experiments[60,61] of the deformed HCP-based materials, which verifies the reliability of results in our work. After the grain reorientation, the basal planes of HCP-Ti will be subjected to tensile loading, and the allotropic phase transformation turns to be the main plastic deformation carriers in the Ti layer.

Interestingly, the transformation of the HCP-Ti to FCC-Ti phase has also been observed. Generally speaking, there are three kinds of orientation relation (OR): (I) $\{0001\}_{\rm HCP}||\{111\}_{\rm FCC}$ and $\langle\bar{1}210\rangle_{\rm HCP}||\langle 110\rangle_{\rm FCC}$;[62,63] (II) $\{10\bar{1}0\}_{\rm HCP}||\{1\bar{1}0\}_{\rm FCC}$ and $\langle 0001\rangle_{\rm HCP}||\langle 010\rangle_{\rm FCC}$;[64,65] (III) $\{10\bar{1}0\}_{\rm HCP}||\{111\}_{\rm FCC}$ and $\langle\bar{1}210\rangle_{\rm HCP}||\langle 110\rangle_{\rm FCC}$. For the first OR, the mechanism of the HCP-Ti to FCC-Ti phase is often supposed to rely on glide of partial dislocations. For the second OR, there is still some controversy about the mechanism: the mechanism of the stress-induced HCP to FCC phase transformation and the pure shuffle mechanism or a shear-shuffle mechanism. For the third OR, the HCP to FCC phase transformation is regarded as the result of the shuffling and shearing of partial dislocation.[66] Figure 8(b) shows the crystallographic orientations between the HCP-Ti twin variant and the FCC-Ti, it is observed that the OR is $\{0001\}_{\rm HCP}||\{111\}_{\rm FCC}$ and $\langle\bar{1}210\rangle_{\rm HCP}||\langle 110\rangle_{\rm FCC}$. When the tension loading is applied to the basal planes of HCP-Ti after grain reorientation, the Shockley partial dislocations with Burgers vectors of the $1/3\langle 10\bar{1}0\rangle$ generate and glide on (0001) plane. As is known to all, the closest-packed stacking sequence of atomic planes is ABABAB$\cdots$, in which the Ti atoms may be designated to lying central points on A-plane, or lying at central points on B-plane. When the first $1/3\langle 10\bar{1}0\rangle$ partial dislocation slips along $\{0001\}$ plane, the atoms in A plane

will rotate 60° with respect to B. The atoms may be located at dot sites on C-plane, forming the stacking sequence of atomic planes ACACAC···, and thus forming one-layer SF of BABABACACA···. As the second $1/3\langle 10\bar{1}0\rangle$ partial dislocation slips along {0001} plane, the atoms in A plane will rotate 60° with respect to C. The atoms may be located at dot sites on B-plane, forming the stacking sequence of atomic planes BCBCBC···, and thus forming two-layer SFs of BABAB**AC**BCBCB···, as shown in Fig. 11(d). With the glide of the partial dislocations along {0001} planes constantly, the three-layer SFs of BABAB**ACB**ABAB··· and four-layer SFs of BABAB**ACBA**CAC··· generate, as shown in Fig. 8(d). This may be the underlying plastic mechanism for the transformation of HCP-Ti to FCC-Ti phase. It should be mentioned that the FCC-Ti has also been observed in simulation[67] and experiments.[9,13,68]

Figure 8(c) shows the crystallographic orientations between HCP-Ti twin variant and the BCC-Ti, and the details of the transformation are presented in Fig. 8(e). The initial 60° between the $\langle 11\bar{2}0\rangle$ directions changes to 70.53° when the tension loading is applied. For the atom stacking sequence of ABABAB··· in HCP structure, the atoms lying in layer A will be stretched and the atoms in layer B will move to the center of the rhombus formed by the atoms in layer A after deformation. Then the {110} plane of BCC structure forms, as shown in Fig. 8(e). The crystallography relation of HCP-Ti and BCC-Ti can be expressed as $\{0001\}_{\rm HCP}||\{111\}_{\rm BCC}$ and $\langle\bar{1}210\rangle_{\rm HCP}||\langle 110\rangle_{\rm BCC}$. The transformations of HCP-Ti and BCC-Ti have also been reported in both simulations[69] and experiment.[70]

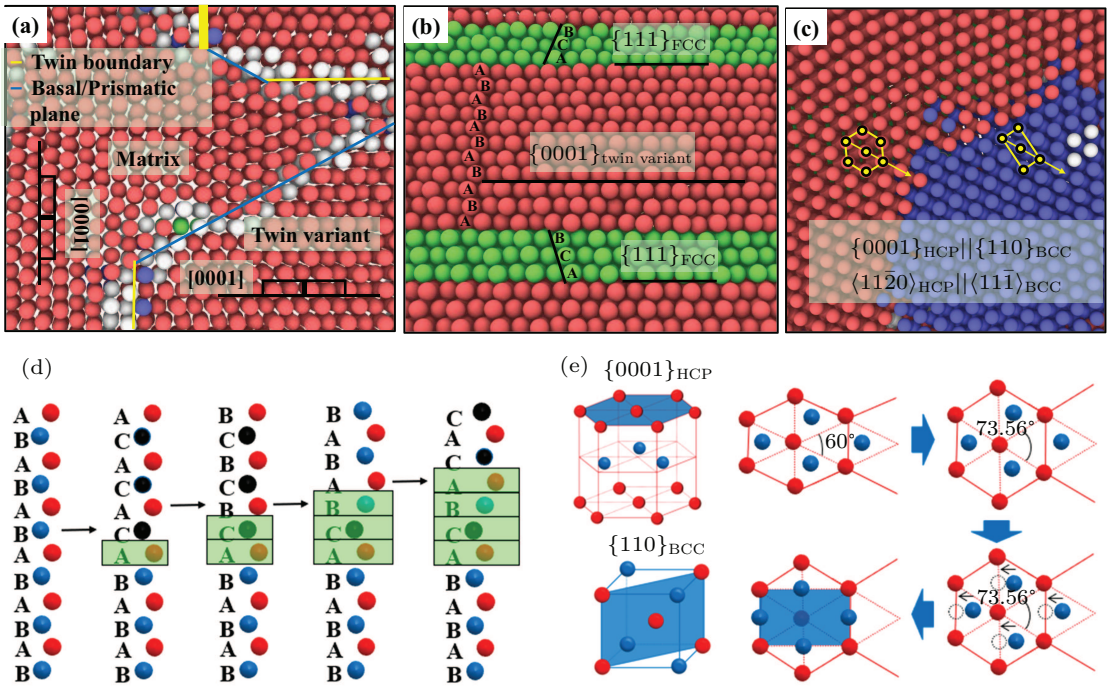


Fig. 8. The details of the deformation carriers presented in crystalline Ti. (a) Crystallographic orientations between the matrix and the twin variant. (b) Crystallographic orientations between the HCP-Ti twin variant and the FCC-Ti. (c) Crystallographic orientations between HCP-Ti twin variant and the BCC-Ti. (d) The mechanism of phase transformation of HCP to FCC structure. (e) Transformation of HCP lattice to BCC lattice.

3.3. Plastic deformation mechanism in amorphous phase

Searching for more details about the crystallization of amorphous TiCu, Fig. 9 shows the shear strain distribution diagram of the Ti/TiCu DPNL with $d = 15.03$ nm at different tensile strains before the first peak stress. Compared with the crystalline part, the atoms in the amorphous layers sustain larger shear strain during the tension. With the increase of tensile strain, the deformed atoms are mainly located at the ACIs, resulting in a noticeable shear strain gradient between the crystalline and the amorphous phase [Figs. 9(a) and 9(c)]. When the tension strain increases to 0.07 [Figs. 9(d) and 9(e)], the BCC atoms in amorphous phase nucleate from the ACIs, which means that the interfaces are beneficial to the crystallization of amorphous TiCu phase. For comparison, the deformation process for the amorphous TiCu phase has also been taken into consideration. However, the plastic deformation is dominated by the generation of uniform STZs, and the amorphous phase does not crystalize into the BCC structure during the tension. This certifies that the crystallization of amorphous TiCu phase is interface-driven behavior. Actually, the ACIs are the soft zones in the Ti/TiCu DPNLs, and the high stress or large shear strain easily concentrates in these regions. During the tension process, the interfaces act as the effective route to release the high stress. That is to say, the high stress is also the driven force for the crystallization of amorphous TiCu alloy. Wang *et al.*[71] reported the structural evolution, i.e., the transformation from amorphous to crystalline structure, during deformation in a work hardenable ductile

TiCu-based bulk metallic glass by high-resolution electron microscopes subjected to large compressive plastic deformation. They believed that the formation of the strip-like crystallite in SBs is possibly due to the effect of both adiabatic heating and shear flow stress. The shear flow stress can result in a flow dilatation of amorphous materials well below glass transition temperature, enhance atomic mobility, and induce the crystallization. This is consistent with the simulation results in this paper.[71] As an important part of many materials such as composite materials and heterojunction structures, interface plays a very important role in the performance regulation, so it has attracted attention of many scholars.[72–75] Specific to the field of crystalline-amorphous interface, the importance of the interface is mainly reflected in the mechanical properties of the structure, especially the plastic deformation ability. Wang *et al.*[15] prepared the Cu/CuZr crystalline/amorphous multilayers and agree that the amorphous–crystal interfaces exhibit unique inelastic shear (slip) transfer characteristics, fundamentally different from those of grain boundaries. That is to say, it plays an important role in the plastic deformation of crystalline/amorphous multilayers. Song *et al.*[74] found that a pronounced interfacial slipping-accommodation mechanism occurs during the plastic deformation with the decreasing amorphous thickness in A/C (CuZr/Cu) nanomultilayers. Cui *et al.*[75] found that local strain concentration at amorphous/crystalline (CuZr/Cu) interface activates the partial dislocation sliding and releases the large atomic shear strain concentration in the amorphous interface.

According to the above conclusions, we want to show more novelty about interface in this work. As mentioned above, we still want to emphasize that the interface can be used as a warehouse to store and release high pressure, and the released pressure can make TiCu undergo structural transformation, which makes it change from amorphous phase to BCC phase. We believe that this has an important effect on the plastic deformation ability of the Ti/TiCu dual-phase nanolaminates.

Searching for more details of the driving force for the crystallization of amorphous TiCu phase, the deformation behaviors of the Ti/TiCu DPNLs at 1 K have been investigated. The results indicate that the crystallization of amorphous TiCu phase is not observed at 1 K, which is different from the result at 300 K. In addition, the influence of layer thickness on the deformation mechanism of Ti/TiCu DPNLs is insignificant, so the representative atomic configurations of the sample with $d = 6.01$ nm at 1 K is presented in Fig. 10. It can be concluded that the crystallization of amorphous TiCu phase is a heat-driven behavior, which is consistent with the experiment results.[76,77] In the tensile process, the stress and heat accumulate constantly near the ACIs. The amorphous phase in the Ti/TiCu DPNLs, which is the soft phase compared with the crystalline part, and make contribution to release the concentration stress and heat. The crystallization is an effective way to change the metastable amorphous state. Therefore, under the synergetic action of heat and stress, the atoms in the amorphous phase rearrange themselves to reduce their chemical potential and transform into stable crystals, then the crystallization generates. The picture in the bottom right corner of Fig. 9 depicts the atomic details after the crystallization in the amorphous phase. It is shown that the {110} plane of the BCC structure is perpendicular to the {0001} plane of the crystalline Ti matrix.

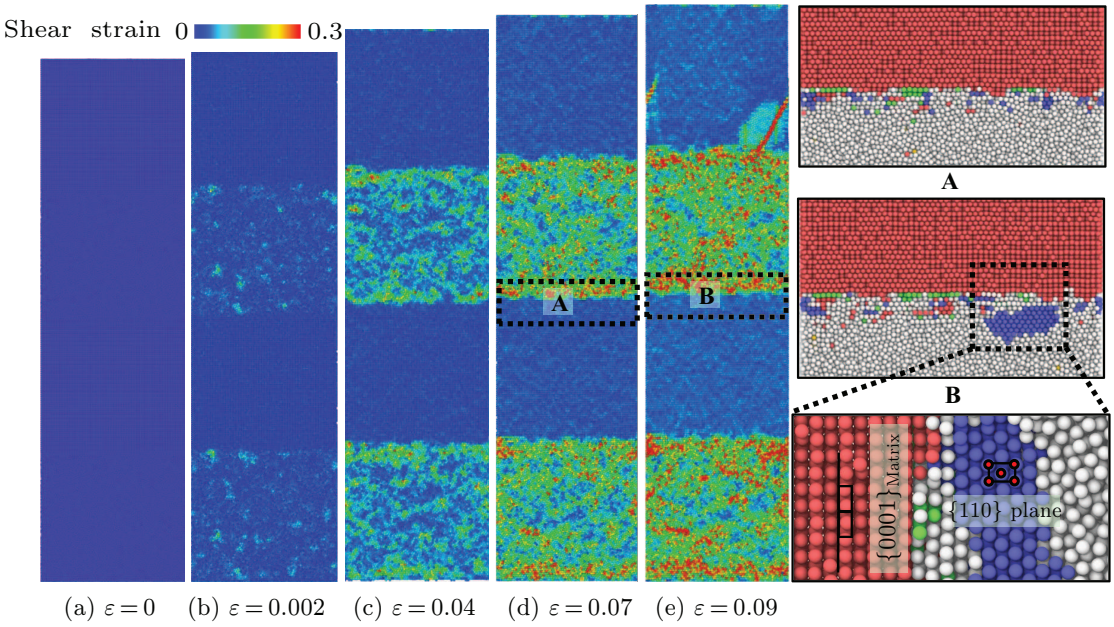


Fig. 9. Shear strain distribution diagram of the Ti/TiCu DPNL with $d = 15.03$ nm at different tensile strains before the first peak stress. The pictures in the top right corner depict enlarged structure of the regions A and B during the tensile process, in which the atomic configuration is analyzed by the CNA method. The picture in the bottom right corner depicts the crystallization details in region B enclosed by rectangle.

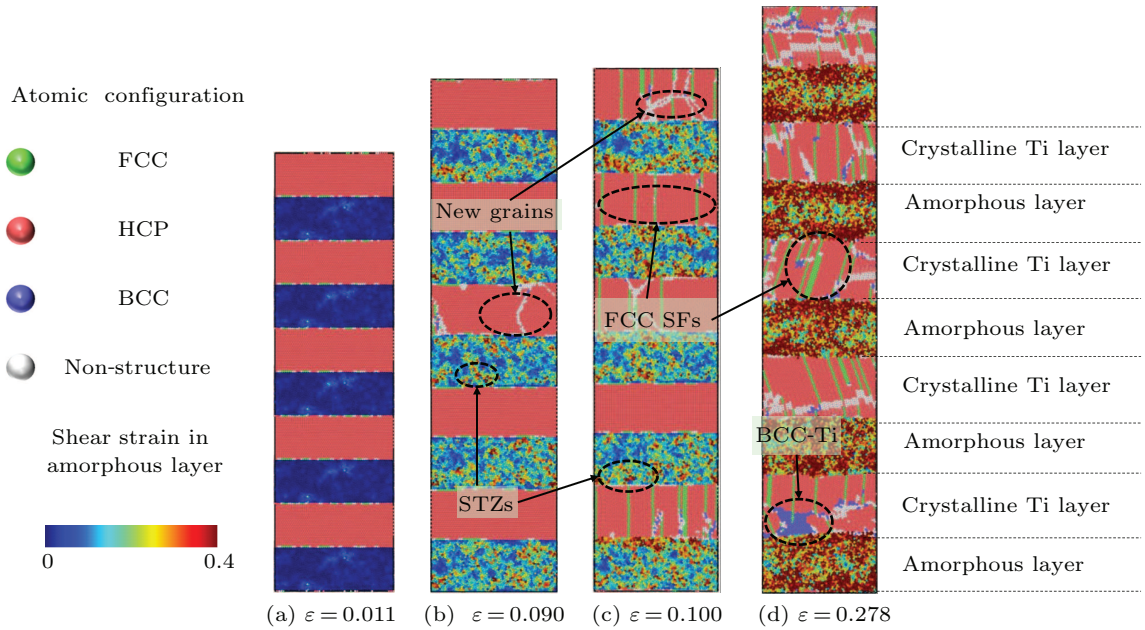


Fig. 10. The atomic configurations of the Ti/TiCu DPNL with $d = 6.01$ nm at different tensile strains at 1 K. In the panel, the atomic configurations of the crystalline layers are analyzed by the CNA method, while the amorphous layers are analyzed by atomic shear strain.

3.4. Size effect on the mechanical behavior of Ti/TiCu DPNLs

In order to verify the universality of the conclusion obtained above, the effect of the sample size on the mechanical behavior of Ti/TiCu DPNLs has also been taken into consideration. Besides the sample size of 5.4 nm × 59.8 nm × 16.4 nm (sample 1) mentioned in Section 2, two larger samples with dimensions of 5.4 nm × 59.8 nm × 24.4 nm (sample 2) and 5.4 nm × 59.8 nm × 40.4 nm (sample 3) are built, which contains ∼ 510000 atoms and ∼ 840000 atoms, respectively. Three models with layer thicknesses of $d = 3.76$ nm, $d = 6.01$ nm and $d = 15.03$ are investigated. According to the stress–strain curves, the effect of sample size on the tensile properties is negligible. The stresses increase linearly with strain up in the elastic stage, while they exhibit a sudden drop after reaching the peak stress. Subsequently, the stresses fluctuate in a large range till to the certain steady values.

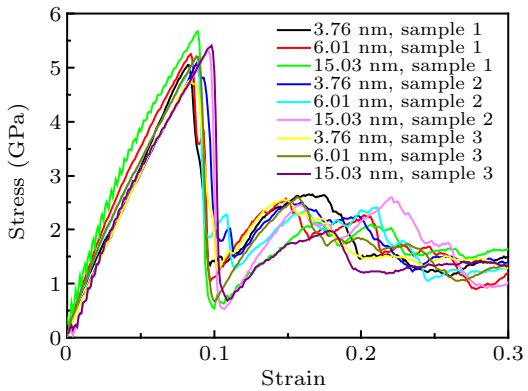


Fig. 11. The typical stress–strain curves of Ti/TiCu DPNLs with different layer thicknesses and sample sizes under tension loading, in which samples 1, 2, and 3 correspond to sizes of 5.4 nm × 59.8 nm × 16.4 nm, 5.4 nm × 59.8 nm × 24.4 nm, and 5.4 nm × 59.8 nm × 40.4 nm, respectively.

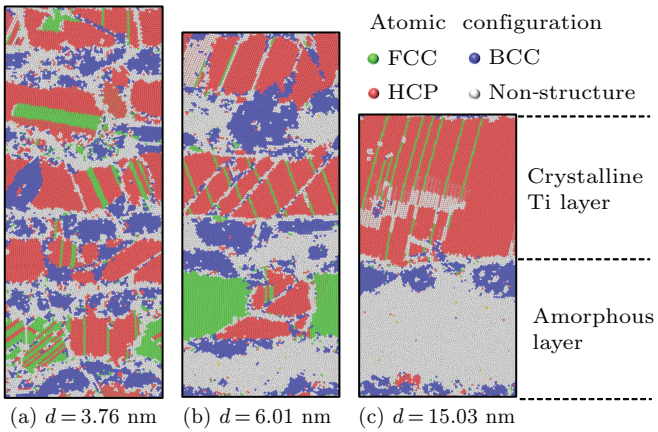


Fig. 12. Atomic configurations of the Ti/TiCu DPNLs with (a) $d = 3.76$ nm, (b) $d = 6.01$ nm, and (c) $d = 15.03$ nm at the strain of 0.3 with sample size of 5.4 nm × 59.8 nm × 24.4 nm.

According to the evolution process of the atomic configuration with different sample sizes, the influence of sample size on the plastic deformation mechanism of Ti/TiCu DPNLs with equal layer thickness is insignificant. The STZs emerge in the amorphous phase in the linear stage of stress–strain curves, as shown in Fig. 11. New grain generates at the crystalline Ti in Ti/TiCu DPNL, which leads to the drop of the stress shown in Fig. 11. The TiCu amorphous phase comes to the plastic stage earlier than the crystalline part. More new grains containing SFs occur in the Ti layers upon further tension loading. The new grains grow up constantly until the grain boundaries are blocked and absorbed by the adjacent ACIs. The transformation of HCP-Ti to FCC-Ti and BCC-Ti has also been observed in the tensile process. Similar to the results in Figs. 3–5, there is no shear band forming in the amorphous layers during the deformation, and the layer thickness affects the degree of crystallization of amorphous TiCu phase in Ti/TiCu DPNLs. The crystalized region of the amorphous TiCu decreases with the

increase of layer thickness. It is observed from Figs. 12 and 13 that in the models with the smallest layer thickness, almost all of the amorphous phase has transformed to crystalline BCC phase; for the models with largest layer thickness, the crystallization of amorphous phase to BCC structure is observed only in the regions near the ACIs; the degree of crystallization for the models with moderate layer thickness is between the former two models.

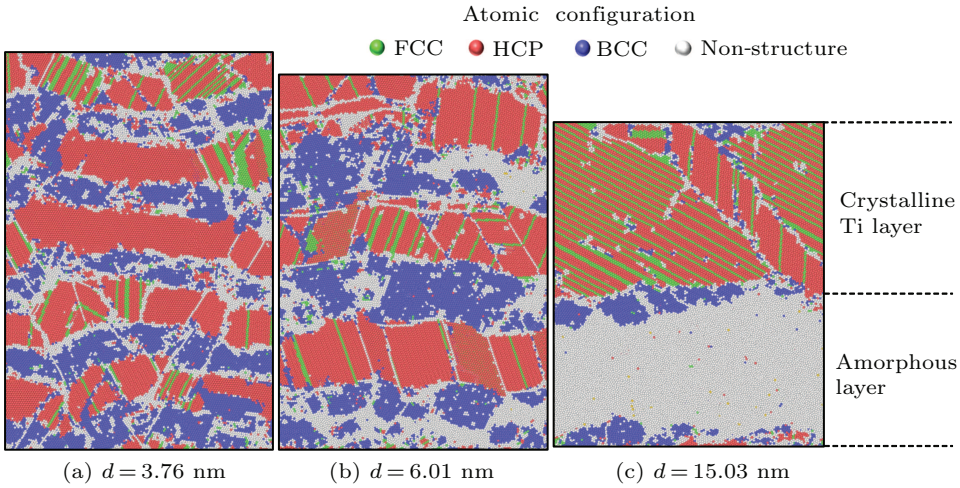


Fig. 13. Atomic configurations of the Ti/TiCu DPNLs with (a) $d = 3.76$ nm, (b) $d = 6.01$ nm, and (c) $d = 15.03$ nm at the strain of 0.3 with sample size of 5.4 nm × 59.8 nm × 40.4 nm.

Furthermore, the mechanical properties and plastic deformation of Ti/TiCu DPNLs under compression have also been investigated in this work. The results indicate that the effect of layer thickness on the peak stress is negligible. The compressive plastic deformation mechanism of Ti/TiCu DPNLs is sensitive to the thickness of crystalline phase. For all the models, the TiCu parts have transformed from the amorphous phase to the BCC structure under high compressive strain,[71] whereas the influence of layer thickness on the crystallization degree of the amorphous phase is not significant. This is different from the results of deformation mechanism under tension loading. For the samples with smaller thickness, the main plastic deformation mechanism of the crystalline phase is the transformation from HCP-Ti to FCC-Ti and BCC-Ti.[9,13,68,70] For the Ti/TiCu DPNLs with larger thickness, the transition from HCP-Ti to FCC-Ti and BCC-Ti and the later transition from FCC-Ti to HCP-Ti dominate the plastic deformation. For the samples with moderate layer thickness, the plasticity deformation of the crystalline part is mainly the transformation from HCP-Ti to FCC-Ti and BCC-Ti, and subsequent transformation from FCC-Ti to HCP-Ti, in which the transformation degree is between the smaller and larger samples.

4. Conclusion

MD simulations are performed to investigate the effect of layer thickness on the mechanical behavior of Ti/TiCu DPNLs in the present work. The simulation results indicate that the influence of the layer thickness on the Young's modulus for the Ti/TiCu DPNLs is apparent, whose values are between the crystalline part and the amorphous part. They are higher than the value obtained by the role of mixture. The plastic deformation for the Ti/TiCu DPNL is dominated by both the amorphous phase and crystalline phase. The layer thickness can hardly affect the plastic deformation mechanism in the crystalline layer, while it influences the plastic deformation mechanism in the amorphous layer. The plastic deformation in the crystalline phase is the grain reorientation, transformation from HCP-Ti to FCC-Ti and BCC-Ti. Nevertheless, the formation of the STZs and the crystallization of the amorphous TiCu are the main plastic deformation in amorphous layers. In addition, the degree of the crystallization is inversely proportional to the layer thickness. The crystallization of the amorphous TiCu is a stress and heat driven process. Furthermore, the effect of sample size on the mechanical behavior and plastic deformation mechanism of Ti/TiCu DPNLs is negligible.

Acknowledgements

Project supported by the National Natural Science Foundation of China (Grant Nos. 51902254 and 12072286), and the Natural Science Foundation of Shaanxi Province, China (Grant Nos. 2021JZ-53 and 2018JQ5108), and the Scientific Research Program Funded by Shaanxi Provincial Education Department, China (Grant No. 20JK0845).

References

[1] Peters M and Leyens C 2003 *Titanium and Titanium Alloys: Fundamentals and Applications* (New York: John Wiley & Sons) pp. 1–35
[2] Zheng G M, Tang B, Zhao S K, Wang W Y, Chen X F, Zhu L and Li J S 2022 *Acta Mater.* **225** 117585
[3] Yuan Z W, Han Y T, Zang S L, Chen J, He G Y, Chai Y, Yang Z F and Fu Q 2021 *Ceram. Int.* **47** 10796
[4] Wang W J, Ji Y C, Fang M X, Wang D, Ren S, Otsuka K, Wang Y Z and Ren X B 2022 *Acta Mater.* **226** 117618
[5] Lu K 2016 *Nat. Rev. Mater.* **1** 16019

[6] Sun L G, Wu G, Wang Q and Lu J 2020 *Mater. Today* **38** 114
[7] Hou Z Q, Zhang J Y, Zhang P, Wu K, Li J, Wang Y Q, Liu G, Zhang G J and Sun J 2020 *Appl. Surf. Sci.* **502** 144118
[8] Wu S H, Hou Z Q, Zhang J Y, Wang Y Q, Wu K, Liu G and Sun J 2019 *Scr. Mater.* **172** 61
[9] Zhang Y F, Xue S, Li Q, Li J, Ding J, Niu T J, Su R, Wang H and Zhang X 2019 *Acta Mater.* **175** 466
[10] Liu Y, Chen Y, Yu K Y, Wang H, Chen J and Zhang X 2013 *Int. J. Plast.* **49** 152
[11] Misra A and Krug H 2001 *Adv. Eng. Mater.* **3** 217
[12] Zhang Y F, Li Q, Gong M, Xue S, Ding J, Li J, Cho J, Niu T, Su R Z, Richter N A, Wang H, Wang J and Zhang X 2020 *Appl. Surf. Sci.* **527** 146776
[13] Zhang Y F, Su R, Niu T J, Richter N A, Xue S, Li Q, Ding J, Yang B, Wang H and Zhang X 2020 *Scr. Mater.* **186** 219
[14] Cao Z H, Sun W, Ma Y J, Li Q, Fan Z, Cai Y P, Zhang Z J, Wang H, Zhang X and Meng X K 2020 *Acta Mater.* **195** 240
[15] Wang Y M, Li J, Hamza A V and Barbee T W 2007 *Proc. Natl. Acad. Sci. USA* **104** 11155
[16] Doan D Q, Fang T H, Tran A S and Chen T H 2020 *J. Phys. Chem. Solids* **138** 109291
[17] Song H Y, Zhang K, An M R, Wang L, Xiao M X and Li Y L 2019 *J. Non-Cryst. Solids* **521** 119550
[18] Zhang K, Song H Y, Deng Q and Li Y L 2020 *J. Non-Cryst. Solids* **534** 119954
[19] Wang Y Q, Liang X Q, Wu K, Zhang J Y, Liu G and Sun J 2018 *Mater. Sci. Eng. A* **732** 29
[20] Wang Y Q, Kiener D, Liang X Q, Bian J J, Wu K, Zhang J Y, Liu G and Sun J 2018 *J. Alloys Compd.* **768** 88
[21] Wang Y Q, Fritz R, Kiener D, Zhag J Y, Liu G, Kolednik O, Pippan R and Sun J 2019 *Acta Mater.* **180** 73
[22] Wang Y Q, Zhang J Y, Liang X Q, Wu K, Liu G and Sun J 2015 *Acta Mater.* **95** 132
[23] Zhang J Y, Wang Y Q, Liang X Q, Zeng F L, Liu G and Sun J 2015 *Acta Mater.* **92** 140
[24] Liang X Q, Zhang J Y, Wang Y Q, Wu S H, Zeng F, Wu K, Liu G, Zhang G J and Sun J 2016 *Mater. Sci. Eng. A* **672** 153
[25] Spindler M, Menzel S B, Eggs C, Thomas J, Gemming T and Eckert J 2008 *Microelectron. Eng.* **85** 2055
[26] Campo K N, Freitas C C D, Lima D D D and Caram R 2020 *J. Mater. Res. Technol.* **9** 15802
[27] Stranak V, Wulff H, Rebl H, Zietz C, Arndt K, Bogdanowicz R, Nebe B, Bader R, Podbielski A, Hubicka Z and Hippler R 2011 *Mater. Sci. Eng. C* **31** 1512
[28] Turnow H, Wendrock H, Menzel S, Gemming T and Eckert J 2016 *Thin Solid Films* **598** 184
[29] Hong S H, Kim J T, Park H J, Kim Y S, Suh J Y, Na Y S, Lim K R, Park J M and Kim K B 2016 *Intermetallics* **75** 1
[30] Kim Y S, Hong S H, Park H J, Kim J T, Jeong H J, Na Y S, Lim K R, Park J M and Kim K B 2017 *J. Alloys Compd.* **707** 87
[31] Chen J, Zhang Z, Yang G, Fang Z, Yang Z, Li Z and He G 2020 *Appl. Surf. Sci.* **513** 145457
[32] Doan D Q, Fang T H and Chen T H 2020 *Tribol. Int.* **147** 106275
[33] Doan D Q, Fang T H and Chen T H 2021 *Sci. Rep.* **11** 1
[34] Lu Y Y, Kotoka R, Ligda J P, Cao B B, Yarmolenko S N, Schuster B E and Wei Q 2014 *Acta Mater.* **63** 216
[35] Su M J, Deng Q, Liu L T, Chen L Y, Su M L and An M R 2021 *Chin. Phys. B* **30** 096201
[36] Wei N, Shi A Q, Li Z H, Ou B X, Zhao S H and Zhao J H 2022 *Chin. Phys. B* **31** 066203
[37] Tian Y Y, Luo G J, Fang Q H, Li J and Peng J 2022 *Chin. Phys. B* **31** 066204
[38] Gu B K, Shen S N and Li H 2022 *Chin. Phys. B* **31** 016101
[39] Tran A S and Fang T H 2021 *Physica E* **126** 114470
[40] Song H Y, Xu J J, Zhang Y G, Li S, Wang D H and Li Y L 2017 *Mater. Des.* **127** 173
[41] Song H Y, An M R, Li Y L and Deng Q 2014 *J. Appl. Phys.* **116** 214305
[42] Song H Y, Yin P, Zuo X D, An M R and Li Y L 2018 *J. Non-Cryst. Solids* **500** 121
[43] Xiao L 2005 *Mater. Sci. Eng. A* **394** 168
[44] Wang Q, Yin Y F, Sun Q Y, Xiao L and Sun J 2014 *J. Mater. Res.* **29** 569
[45] Su M J, Deng Q, An M R, Liu L T and Chen L Y 2021 *J. Alloys Compd.* **868** 159282
[46] Plimpton S 1995 *J. Comput. Phys.* **117** 1
[47] Wadley H N G, Zhou X, Johnson R A and Neurock M 2001 *Prog. Mater. Sci.* **46** 329
[48] Zhou X W, Wadley H N G, Johnson R A, Larson D J, Tabat N, Cerezo A, Petford-Long A K, Smith G D W, Cliftond P H, Martens R L and Kelly T F 2001 *Acta Mater.* **49** 4005
[49] Tian Y Y, Li J, Hu Z Y, Wang Z P and Fang Q H 2017 *Chin. Phys. B* **26** 126802
[50] Chen S D, Ke F J, Zhou M and Bai Y L 2007 *Acta Mater.* **55** 3169
[51] Faken D and Jónsson H 1994 *Comput. Mater. Sci.* **2** 279
[52] Shimizu F, Ogata S and Li J 2007 *Mater. Trans.* **48** 2923
[53] Stukowski A 2009 *Model. Simul. Mater. Sci. Eng.* **18** 015012
[54] Ashby M F 1993 *Acta Metall. Mater.* **41** 1313
[55] Zhu X Y, Liu X J, Zeng F and Pan F 2010 *Trans. Nonferr. Metal. Soc.* **20** 110
[56] Su M J, Deng Q, An M R, Liu L T and Ma C B 2019 *Comput. Mater. Sci.* **158** 149
[57] Greer A L and Ma E 2007 *MRS Bull.* **32** 611
[58] An M R, Deng Q, Li Y L, Song H Y, Su M J and Cai J 2017 *Mater. Des.* **127** 204
[59] Ren J Q, Sun Q Y, Xiao L, Ding X D and Sun J 2014 *Comput. Mater. Sci.* **92** 8
[60] Liu B Y, Wang J, Li B, Lu L, Zhang X Y, Shan Z W, Li J, Jia C L, Sun J and Ma E 2014 *Nat. Commun.* **5** 3297
[61] Sun Q, Zhang X Y, Ren Y, Tu J and Liu Q 2014 *Scr. Mater.* **90–91** 41
[62] Zhao H L, Hu X Y, Song M and Ni S 2017 *Scr. Mater.* **132** 63
[63] Yu Q, Kacher J, Gammer C, Traylor R, Samanta A, Yang Z Z and Minor A M 2017 *Scr. Mater.* **140** 9
[64] Hong D H, Lee T W, Lim S H, Kim W Y and Hwang S K 2013 *Scr. Mater.* **69** 405
[65] Wu H C, Kumar A, Wang J, Bi X F, Tomé C N, Zhang Z and Mao S X 2016 *Sci. Rep.* **6** 24370
[66] Chen P, Wang F X and Li B 2019 *Acta Mater.* **171** 65
[67] An M R, Su M J, Deng Q, Song H Y, Wang C and Shang Y 2020 *Chin. Phys. B* **29** 046201
[68] Yang J X, Zhao H L, Gong H R, Song M and Ren Q Q 2018 *Sci. Rep.* **8** 1992
[69] An M R, Song H Y, Deng Q, Su M J and Liu Y M 2019 *J. Appl. Phys.* **125** 165307
[70] Wang Q Q, Liu Z Q, Wang B and Mohsan A U H 2017 *Mater. Sci. Eng. A* **690** 32
[71] Wang G, Liu Y H, Yu P, Zhao D Q, Pan M X and Wang W H 2006 *Appl. Phys. Lett.* **89** 251909
[72] He Y, Hu S M, Zhu W L and Ouyang G 2020 *J. Phys. D: Appl. Phys.* **53** 125101
[73] Zhao Y P, Tan S L and Ouyang G 2021 *J. Phys. D: Appl. Phys.* **54** 145107
[74] Song H Y, Wang M, Deng Q and Li Y L 2018 *J. Non-Cryst. Solids* **490** 13
[75] Cui Y, Shibutani Y, Li S, Huang P and Wang F 2017 *J. Alloys Compd.* **693** 285
[76] Zhang Y Y, Lin X, Gao X H, Su X L, Luo S B and Huang W D 2021 *Intermetallics* **136** 107256
[77] Song K K, Han X L, Pauly S, Qin Y S, Kosiba K, Peng C X, Gong J H, Chen P X, Wang L, Sarac B, Ketov S, Mühlbacher M, Spieckermann F, Kaban I and Eckert J 2018 *Mater. Des.* **139** 132